EurJOC
European Journal of Organic Chemistry

Research Article
doi.org/10.1002/ejoc.202201453

Chemistry Europe
European Chemical Societies Publishing

www.eurjoc.org

VIP *Very Important Paper*

Special Collection

Strapped Porphyrins as Model Systems for Atropisomeric Photosensitizer Drugs

Claire Donohoe,[a, b] Asterios Charisiadis,[c] Sophie Maguire,[c] Brendan Twamley,[d] Fábio A. Schaberle,[b] Lígia C. Gomes-da-Silva,*[b] and Mathias O. Senge*[a, c]

The time dependence of atropisomer interconversion has limited the pursuit of single atropisomer drug candidates, even in circumstances where one atropisomer presents favorable biological activity over another. Moderate interconversion energy barriers risk compromising drug stability. As a result, examples of atropisomerically pure drugs in current clinical use are rare. However, in recent years, there has been a shift towards the development of single, stable atropisomer drug candidates with enhanced activity. Consequently, development of methods which effectively restrict rotation in a configuration which favors activity is highly beneficial. The picket fence porphyrin α_4 atropisomer configuration has been previously demonstrated to improve the cell internalization of the pre-clinical drug, redaporfin, applied in photodynamic therapy. In this work, the α_4 configuration was modelled with novel porphyrin photosensitizers through strapped moieties which effectively fixed the atropisomeric configuration. The stable *cis*-$\alpha\alpha$ configuration demonstrated enhanced cell membrane permeation, effectively predicting the behavior of the α_4 configuration and indicates that strapped porphyrins can serve as stable model systems for the investigation of photoactive drugs.

Introduction

An intrinsic issue for atropisomeric drugs is the time dependence of interconversion with dramatically different racemization half-lives ranging from minutes to years. With the potential to undermine the efficacy and production of stable drug substances, it is perhaps unsurprising that atropisomerism has been dubbed a 'lurking menace' for drug development.[1] Even atropisomers with large interconversion barriers ($\geq$ 30 kcal.mol^{-1}), considered class 3 atropisomers, require careful evaluation.[2] As with chiral stereoisomers, pre-clinical assessment of atropisomer drug candidates generally involves consideration of atropisomer pharmacokinetic profiles due to the potential racemization of pure isomers upon metabolism.[1] In cases where an individual atropisomer presents a favorable biological activity, alterations to molecular structure which increases rotational barriers in a manner that preserves metabolic stability are highly desirable.

A prevalent strategy to improve stability involves an increase of steric bulk around the atropisomer axis.[2] Additionally, there are cases where a rotating axis interconversion energy barrier can be increased through creation of a bridge.[3] For photodynamic therapy, a specific tetrapyrrole atropisomer configuration, the α_4 atropisomer, was previously identified to increase cellular internalization and consequently enhanced phototoxicity in vitro and in vivo.[4] The source for this varied efficacy was rationalized in terms of the atropisomer molecular structure, with the distribution of polar substituents oriented to one side of the macrocycle plane, enhancing interaction with the cell-membrane and improving passive permeation. In the present work, restrictive strap moieties were used in novel porphyrin photosensitizers to enforce an α_4 configuration (Figure 1) while effectively locking the axis of rotation for enhanced stability.

Strapped porphyrins feature covalent connections between either β-β- [5] or meso-meso-[6] positions of the porphyrin macrocycle.[7] These systems were originally developed to gain understanding of the structure and activity of biologically active sites. The domed shape of deoxyhemoglobin, known to feature as part of the heme protein, was pursued.[8] Linkage at phenyl substituents of 5,10,15,20-tetraphenylporphyrins gave rise to a variety of strapped porphyrin shapes with names derived from

[a] C. Donohoe, Prof. Dr. M. O. Senge
Medicinal Chemistry
Trinity Translational Medicine Institute
Trinity Centre for Health Sciences
St. James's Hospital, Trinity College Dublin
The University of Dublin
Dublin 8, (Ireland)
[b] C. Donohoe, Dr. F. A. Schaberle, Dr. L. C. Gomes-da-Silva
CQC, Coimbra Chemistry Centre
University of Coimbra
Coimbra 3004-535 (Portugal)
E-mail: ligia.silva@uc.pt
[c] Dr. A. Charisiadis, S. Maguire, Prof. Dr. M. O. Senge
School of Chemistry
Chair of Organic Chemistry
Trinity Biomedical Sciences Institute
Trinity College Dublin
The University of Dublin
152-160 Pearse Street, Dublin (Ireland)
E-mail: sengem@tcd.ie
https://www.sengegroup.eu/
[d] Dr. B. Twamley
School of Chemistry, Trinity College Dublin
The University of Dublin, Dublin 2 (Ireland)

Supporting information for this article is available on the WWW under https://doi.org/10.1002/ejoc.202201453

Special Collection *Part of the "Board Member" Virtual Special Collection*

Research Article
doi.org/10.1002/ejoc.202201453

Chemistry Europe
European Chemical Societies Publishing

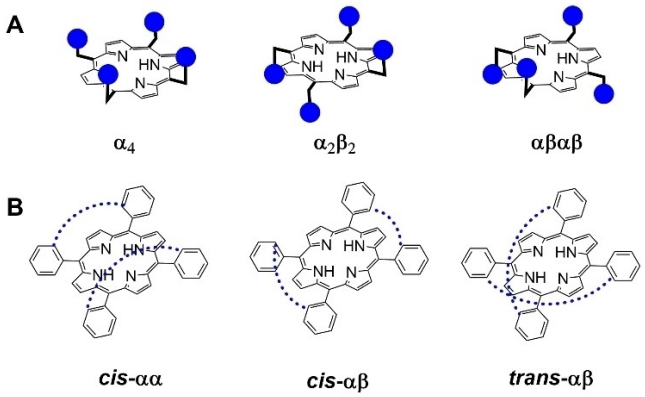

Figure 1. Configurations of (A) picket-fence porphyrin atropisomers and (B) double strapped porphyrin isomers.

macroscopic objects including 'capped porphyrins' and double strapped 'basket handle' porphyrins.[9] Investigation of biomimetic models was dominated by the pursuit to induce porphyrin distortion.[10] This was successfully achieved by Dolphin's group, with the preparation of a β-β-single strapped porphyrin by acid catalyzed cyclization of bis-dipyrromethane.[10b] Single strapped meso-linked porphyrins were also prepared to target a cytochrome c oxidase model by Wytko et al. through condensation between a dipyrromethane and dialdehyde.[11] However, a more accurate model was later obtained with a double strapped porphyrin through post-functionalization of porphyrin atropisomers with linkers.[12] Strapped porphyrins have featured in areas beyond biomimetic models as chiral catalysts[13] and scaffolds in molecular engineering[14] as well as potential oxygen storage devices with anthracene straps.[15]

Photodynamic therapy (PDT), which effectively combines a photosensitizer drug, light of a specific wavelength and molecular oxygen to mediate a oxidative therapeutic effect, tend to feature the tetrapyrrole motif.[16] However, examples of strapped porphyrins as photosensitizers (PSs) are limited. Regardless of the synthetic route selected, isolation and preparation of stereoisomerically pure strapped porphyrins in reasonable yield remains a challenge.[17] In addition to low synthetic yields, the lack of investigation may be partly due to the primary focus of these systems generally involving macrocycle distortion. With short strap lengths, a non-planar conformational change may occur which quenches fluorescence quantum yields.[18] Macrocycle distortion may also lead to reduced singlet oxygen quantum yield generation,[19] a property detrimental to photodynamic therapy efficacy. Therefore, strap length for integration in PSs must be tuned to ensure planarity. Glycosyl containing single strapped porphyrins have been studied as PSs and compared to hematoporphyrin derivative. The porphyrins were prepared by a BF_3 catalyzed direct condensation of a dipyrromethane and dialdehyde. A mixture of 5,10- and 5,15-single strapped porphyrins were derived with the latter showing enhanced phototoxicity in vitro.[20] Double strapped systems, specifically calix[4]pyrroles, have been demonstrated to act as synthetic transmembrane carriers with the *cis*-αα configuration providing a suitable aromatic cavity for proline transport.[21] The potential for these systems to enhance cellular uptake is high. Despite potentially low yields, interest in strapped porphyrin synthesis continues[22] alongside their role as heme models.[23]

In this work, we introduced strapped linkages to porphyrins intended to alter membrane passage. Alkyl and phenyl straps were used to lock rotation of three meso-tetraarylporphyrins and to form double strapped porphyrins. These strapped porphyrins have linkages at the 5,10- and 15,20-meso-positions which direct meso-aryl substituents above or below the macrocycle plane. Depending on strap orientation, they are referred to as *cis*-αα, *cis*-αβ and *trans*-αβ. Such isomers are analogous in configuration to porphyrin atropisomers, α_4, $\alpha_2\beta_2$ and αβαβ, respectively (Figure 1). Polar aryl substituents were incorporated to double strapped porphyrin design to achieve enhanced membrane permeation for the *cis*-αα isomer. Direct condensation methods were employed to pursue both *cis*-isomers for in vitro comparison. Structural elucidation was assisted through a combination of NMR spectroscopy and single-crystal X-ray crystallography. Photophysical studies provided insight into the relative planarity between isomers. Membrane passage was determined in two cell lines with the *cis*-αα isomer exhibiting preferential uptake, illustrating the advantage of the α_4 motif to enhance internalization.

Results and Discussion

Strapped Porphyrin Synthesis

Double strapped porphyrins were prepared using a direct condensation reaction between a dialdehyde and pyrrole. This approach was favored to ensure *cis*-isomers were the major product,[9] as we aimed to investigate whether the locked *cis*-αα configuration, an analogue of redaporfin α_4, conferred an advantage in membrane passage over other isomers. Linker straps were selected with two requirements. Firstly, the length of the strap needed to be long enough to ensure an absence of macrocycle distortion. Such distortion is inversely proportional to linker length.[8,24] Porphyrin planarity was pursued due to the decrease in singlet oxygen generation which tends to occur with distorted porphyrin macrocycles,[19] inhibiting PS potential.[25] Secondly, it was necessary to ensure that strap length was short enough to prevent flexible s-shaped straps and free rotation.[9] Additionally, the strap chosen was hydrophobic in order to induce amphipathic behavior in the case of *cis*-αα, with hydrophobic straps on one side of the macrocycle and polar hydrogen bonding groups on the other. The stability of an alkyl chain strap was first targeted with a hexyl chain. This strap was previously used for double strapped porphyrin preparation in the absence of distortion by the Lindsey group with *o,o'*-linked straps. Increase of an alkyl strap length to eight carbons or more was proposed to lead to undesirable, flexible s-shaped conformations.[9]

Research Article
doi.org/10.1002/ejoc.202201453

A series of dialdehydes were prepared by alkylation of the appropriate commercially available salicylaldehyde derivative; 5-nitrosalicylaldehye or 5-(methoxycarbonyl)salicylaldehyde, according to the procedure of Scheme 1. The alkylation method was adapted from Charisiadis et al.[26] and featured activation of the salicylaldehyde derivative precursor by stirring for 1 h in the presence of K_2CO_3 in DMF prior to the addition of the brominated linker. Dialdehydes **1**–**3** were obtained in adequate yields, suitable for multigram condensation. Similar linker types have been prepared by Wagner et al.[9] and Reddy et al.[27] with comparable yields.

A common obstacle for the preparation of double strapped porphyrin *cis*-isomers is low yields. This was somewhat met by the one-flask synthesis developed by the group of Lindsey.[28] However, the alkyl linker dialdehyde **1** demonstrated limited solubility in solvents acceptable for this strategy including CH_2Cl_2 or $CHCl_3$. As a result, condensation was first attempted using adapted Adler-Longo conditions[29] of refluxing dialdehyde and pyrrole in propionic acid, originally optimized for direct condensation of pyrrole and dialdehyde by Momenteau et al.[30] Conditions are shown in Scheme 2. After 3 h of heating at 150 °C, purification by chromatography to remove pyrrole impurities proceeded. A mixture of three porphyrins was indicated by TLC. The combined porphyrin yield was inadequate (< 0.5 %) to allow complete characterization following separation. Mass spectrometry analysis (MALDI) indicated that each fraction corresponded to the mass of the targeted strapped porphyrin **4** (Scheme 2). In an attempt to improve the yield, Lindsey conditions[9] were used with high dilution. Marginally greater solubility of dialdehyde **1** was observed in CH_2Cl_2 over $CHCl_3$ and was, thus, selected for condensation with $BF_3 \cdot OEt_2$ as a catalyst. After 24 h stirring at rt under argon, DDQ was added as an oxidation step and neutralized with TEA. Two fractions were separated by chromatography.

Characterization confirmed that two strapped porphyrin **4** isomers were obtained using the Lindsey conditions. A low isolated yield (< 1%) in comparison to similar *o,o'*-linked strapped porphyrins (15 %) was attained.[9] This was likely caused by the low solubility of the dialdehyde **1** in CH_2Cl_2 which led to incomplete condensation of starting material. This was apparent from a dialdehyde peak visible at 10.3 ppm in ^{1}H NMR following porphyrin separation, contaminating the *cis*-αα-**4** porphyrin. The low solubility of the dialdehyde **1** across a variety of organic and aqueous solvents prevented chromatographic purification of the porphyrin. Metalation with zinc using $Zn(OAc)_2$ in CH_2Cl_2 sufficiently altered the porphyrin polarity relative to the dialdehyde **1** to allow recrystallization from ethyl acetate. The pure Zn-porphyrin **4** subsequently underwent demetallation with TFA to yield the *cis*-αα-**4**. Dialdehyde solubility limited condensation and ultimately led to extensive purification steps which likely contributed to a reduced yield.

Elucidation of the strapped porphyrins **4** configuration was possible due to ^{1}H NMR and single-crystal X-ray crystallography. Mass spectrometry (MALDI) analysis and absorption spectra were identical for both strapped porphyrin fractions following separation. The order of elution of similar double strapped porphyrins on silica gel has previously been reported as *trans*-αβ followed by *cis*-αβ and *cis*-αα.[17,30] For the two porphyrin fractions prepared using Lindsey conditions, retention factors aligned with the latter fraction of the Adler-Longo condensation on TLC. This suggested that the two porphyrins were the *cis*-isomers, which conforms with the almost exclusive formation observed by the Lindsey group during method development for the condensation.[9] While the ^{1}H NMR spectra of the alkyl

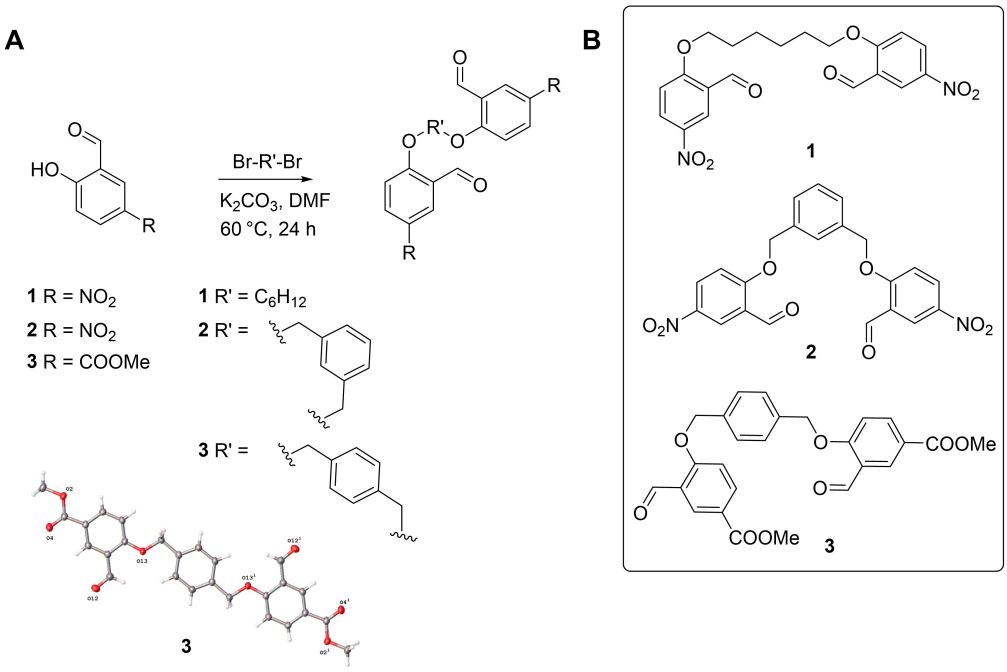

Scheme 1. (A) Synthesis of dialdehydes. (B) Target dialdehydes for strapped porphyrin preparation and view of the molecular structure of **3** in the crystal.

Research Article
doi.org/10.1002/ejoc.202201453

Chemistry Europe
European Chemical Societies Publishing

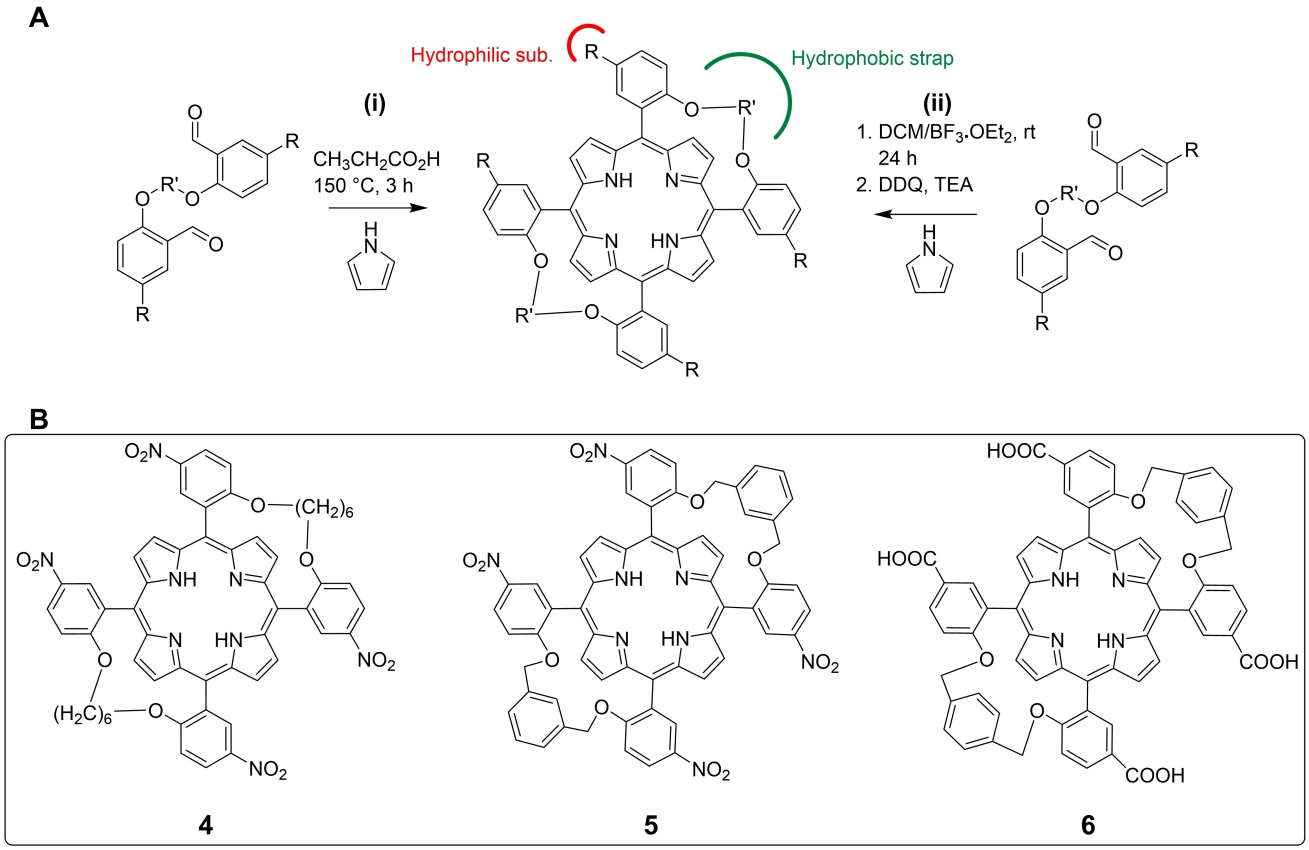

Scheme 2. (A) Condensations of dialdehyde and pyrrole to prepare double strapped porphyrins via the (i) Adler-Longo and (ii) Lindsey condensation methods. (B) Target strapped porphyrins.

strap porphyrins (Figure S4 and S5) were similar, they displayed distinctive resonances for β-pyrrolic protons. The first fraction displayed eight magnetically equivalent β protons as a singlet. This is generally a feature more consistent with the *trans*-αβ symmetry.[27,30] However, the methylene protons of the hexyl strap did not exhibit the characteristic upfield shift associated with the diamagnetic anisotropy typical of *trans* configurations.[31] The second fraction β-pyrrolic protons split into two singlet resonances in agreement with anticipated symmetry of the *cis*-αα configuration.[30] However, ^{1}H NMR could not ambiguously distinguish the two isomers' configuration alone.

Alkyl-strapped porphyrin configurations were both confirmed as *cis*-isomers by single-crystal X-ray crystallography. Crystals were grown from the chromatographic fractions and structures could be conclusively assigned as *cis*-αβ for the first fraction to elute and *cis*-αα for the second (Figure 2, Figure S13A,B and Table S1). The order of elution was in agreement with literature sources.[17,27,30] The *cis*-αβ-**4** isomer porphyrin core adopted a primarily planar conformation (Figure 2A). The asymmetric unit was identified as two unique half molecules. The *cis*-αα-**4** isomer (Figure 2B) showed slight saddle deformation. Crystallization occurred as one complete molecule which was highly disordered at both 1,6-bis(4-nitrophenoxy)hexane substituents. Lattice voids were partially occupied by hexane solvent molecules. The intramolecular hydrogen bonding distances between the pyrrole macrocycle

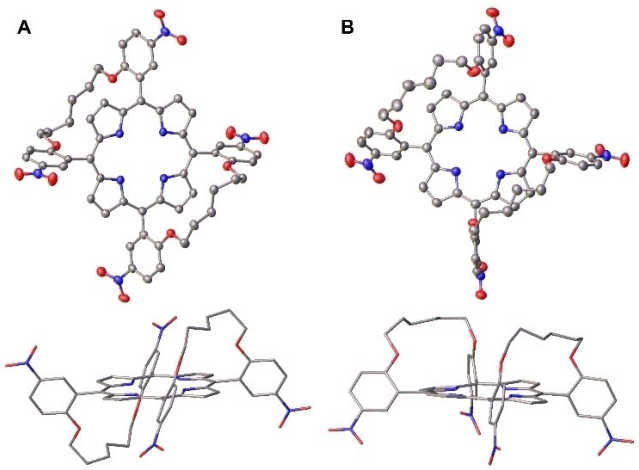

Figure 2. View of the molecular structure in the crystal of (A) *cis*-αβ-**4** and (B) *cis*-αα-**4** isomers with plan (atomic displacements at the 50% probability level) and side views (schematic pipe view for clarity). (A) Symmetry generated complete molecule of *cis*-αβ-**4** from one of the unique half molecules of the asymmetric unit. (B) *cis*-αα-**4** molecular structure with hexane solvent omitted. Major occupied moiety of each isomer represented only and hydrogen atoms are omitted for clarity.

Research Article
doi.org/10.1002/ejoc.202201453

Chemistry Europe
European Chemical Societies Publishing

subunits were identical for the *cis*-αβ-**4** isomer as 2.31 Å. The *cis*-αα-**4** isomer showed small deviation between the two bonding distances, 2.33 and 2.31 Å, respectively, consistent with the observed minor deformation. Crystal packing is presented in Figure S13. Interconversion of the straps at rt was not observed in solution by ^{1}H NMR over approximately one week and the isomer configuration assigned to each fraction were the sole components of each.

To improve the double strapped porphyrin yield, dialdehydes with greater solubility under condensation conditions were pursued with phenyl-linked dialdehydes **2** and **3** (Scheme 1). A more rigid strap linker was anticipated to lead to improved strapped porphyrin yields.[9] Both dialdehydes were acquired with similar success to dialdehyde **1** but enhanced chloroform solubility was observed. This facilitated the Lindsey condensation method with dialdehyde **2**. Selective porphyrin isomer formation was indicated by TLC after condensation and an initial column chromatography to remove pyrrole impurities. ^{1}H NMR analysis indicated a single double strapped porphyrin with a *cis* configuration due to two characteristics (Figure S6); β-pyrrolic protons were observed as two singlet signals. Additionally, the splitting observed for methylene proton peaks at 5.67 and 5.00 ppm, correlated to an equivalent ^{13}C resonance at 71.79 ppm by HSQC (Heteronuclear Single Quantum Coherence) analysis. Thus, these methylene carbons were indicated to be potentially orientated in the same environment relative to the macrocycle plane as a *cis*-αα isomer.

Selective formation of a single double strapped porphyrin is unlikely. The Lindsey group[9] was confronted by the same issue during the preparation of a series of *m,m'*-linked strapped porphyrins. They discovered through ^{1}H NMR analysis that the porphyrins were rapidly interconverting. This was unlikely to be the case with strapped-porphyrin **5**, as the Lindsey group had only observed interconversion with longer alkyl strap units.[9] Therefore, it may be possible that the other isomer formed but to such a lower extent that it was not possible to isolate during purification. The preferred formation of *cis*-αα over *cis*-αβ has been previously established, initially by Momenteau et al.[30] for the Adler-Longo condensation and later confirmed for the Lindsey condensation method by the Lindsey group.[9]

The use of the rigid linker in dialdehyde **2** proved beneficial for the Lindsey condensation with an isolated yield of 8.1%. In order to prepare the other isomer, the Adler-Longo condensation method was employed. Three strapped porphyrins were indicated by TLC (Table 1). Repetitive chromatography purification was required to isolate the three fractions. A substantially lower combined yield, 1.25%, was observed for this procedure. The elution order, previously established for porphyrins with similar straps[27] and comparison of ^{1}H NMR, confirmed the dominant Lindsey condensation product as *cis*-αα. The ^{1}H NMR of *trans*-αβ-**5** (Figure S8) indicated the characteristic features of symmetry associated with *trans* double strapped porphyrins, such as eight magnetically equivalent β-pyrrolic protons and shielding of the strap's methylene protons due to its position stretching the porphyrin plane.[31] Both *cis*-isomers were formed in a higher proportion with respect to the *trans*-αβ, a common outcome of these reaction conditions.[30]

Table 1. Synthesis of double strapped porphyrins.

Dialdehyde	Strapped porphyrin	Condensation Conditions	No. of porphyrins by TLC	Isolated comb. yield [%]
1	**4**	Adler-Longo	3	<0.5
1	**4**	Lindsey	2	<1.0
2	**5**	Lindsey	1	8.14
2	**5**	Adler-Longo	3	1.25
3	**6**	Lindsey	1	1.30
3	**6**	Adler-Longo	2	0.5

The stability of the strapped-porphyrin *cis*-αα-**5** isomer was probed. The *cis*-αα isomer was selected due to the lower thermal stability observed by Urbani et al.[17] An initial attempt was made to induce strap rotation through heating a sample of the strapped porphyrin for 24 h in toluene at 111 °C. However, no conversion was observed. Subsequent attempts in DMF (153 °C) and DMSO (189 °C) lead to no observable conversion by TLC. The strapped porphyrin was deemed stable against conversion at elevated temperatures.

The number of double strapped porphyrins formed varied depending on the condensation protocol employed (Table 1). Lindsey condensation conditions resulted in formation of only *cis* configurations. The Adler-Longo reaction yielded the *cis* configuration with preference over *trans* isomer formation.[30] This trend, which conforms with similar strapped systems in the literature, has prompted alternative preparative strategies specific to the *trans* isomer including post-functionalization of the porphyrin with the strap[30] or condensation between a bis-dipyrromethene and dialdehyde.[15] In both the Lindsey and Adler-Longo condensations, the *cis*-αα isomer dominated, consistent in the preparation of double strapped porphyrins with both respective strategies in this work.[9,30]

A consistent issue encountered with the isolation of each strapped porphyrin was low solubility across a variety of solvents, which hindered characterization during preparation. TFA was employed to solubilize all porphyrins for ^{1}H NMR analysis via dication salt formation. A new double strapped porphyrin **6** was targeted in an attempt to improve solubility. The strap length of dialdehyde **2** was increased to attempt to alter the number of porphyrins accessible from the Lindsey condensation. However, Adler-Longo conditions were necessary to form multiple porphyrins: *cis*-αα-**6** and *trans*-αβ-**6**. The strapped porphyrin *cis*-αβ-**6** was not observed to form. Carboxylic acid functionality was introduced by hydrolysis using KOH as a base of methyl-ester groups following condensation. The solubility of the novel porphyrins was significantly higher than that of strapped porphyrins **5**. Structural characterization of strapped porphyrins **6** was confirmed by single-crystal X-ray crystallography (Figure 3, Figure S13C,D and Table S1). Saddle distortion[32] of the porphyrin macrocycle was apparent with the COOMe-*trans*-αβ-**6** isomer.

Research Article
doi.org/10.1002/ejoc.202201453

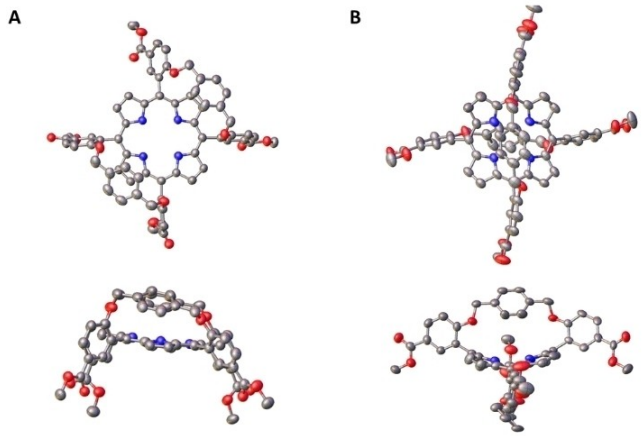

Figure 3. View of the molecular structure in the crystal of (A) COOMe-*cis*-αα-**6** with CH_2Cl_2 solvent omitted and (B) COOMe-*trans*-αβ-**6** with symmetry generated complete molecules from the unique half molecules of the asymmetric unit. Major disordered moiety of each isomer represented. Atomic displacements at the 50% probability level and H atoms are omitted for clarity.

Strapped porphyrin photophysical and photochemical characterization

Evaluation of the photophysical properties of the double strapped porphyrins provided valuable insight into the relative planarity of strapped porphyrin isomer macrocycles. Results are presented in Table 2 and Figure S14.

Strapped porphyrins **4** with moderate length, hexyl straps were indicated by single-crystal X-ray crystallography to share a lack of significant distortion. Overlapping absorption spectra (Figure S14) confirmed that there were no major changes in the porphyrin macrocycle conformation between the isomers which would alter photophysical properties. If macrocycle distortion was present, a bathochromic shift would be anticipated.[8,19] The *cis*-isomers of strapped porphyrin **5** also exhibited overlapping absorption spectra with the Soret band (λ_{Soret}) at 428 nm; however, the *trans* isomer demonstrated a bathochromic shift of 10 nm to 434 nm. This would indicate that when the phenyl straps of porphyrin **5** are linked between positions 5,15 and 10,20, some distortion is introduced to the porphyrin macrocycle. A similar shift was observed for the *trans*-αβ-**6** isomer, indicating distortion, which was confirmed by single-crystal X-ray crystallography (Figure 3B). The propensity of these rigid linkers to induce slight distortion has previously been observed by Reddy et al.[27]

An accompanying indication of distortion was not only a bathochromic shift but significant reduction in molar absorptivity. With the introduction of a rigid linker in strapped porphyrins **5** and **6**, lower molar absorption coefficients were observed relative to strapped porphyrins **4**; however, this was particularly the case for *trans*-αβ-**5** and *trans*-αβ-**6** isomers. Reddy et al.[27] rationalized the changes by deviations in the intensity of Soret and Q bands, specifically with a *trans*-αβ isomer, due to changes in degeneracy of the π-molecular orbitals of the porphyrin ring, resulting in red shifts and a significant decrease in intensity. Fluorescence quenching tends to accompany these signs of distortion for absorption spectra.[18] Indeed, the absolute values of fluorescence quantum yield (Table 2, Φ_F) of the double strapped porphyrins *cis*-αβ-**5** and *trans*-αβ-**6**, recorded using an integrating sphere, were both lower relative to the respective *cis*-αα isomers.

The consequences of distortion for the *trans*-αβ-**6** were apparent with a slightly lower singlet oxygen quantum yield (Table 2, Φ_Δ) value. A decrease in singlet oxygen quantum yields has been established as relevant to the planarity of the porphyrin macrocycle.[19] Determination of the singlet oxygen quantum yield was performed by employing two methods: steady-state and time-resolved techniques to detect phosphorescence emission from singlet oxygen. The main difference between these techniques is the use of continuous (CW) or pulsed light to induce excited states of the molecules. The values of Φ_Δ of *trans*-αβ-**6** and *cis*-αα-**6** presented are the average of three independent measurements using either technique. For strapped porphyrins **4**, the steady-state method gave values slightly higher than 1 and the pulsed method values ca. 1.3 (not shown in Table 2). The increase of the Φ_Δ value obtained using pulsed laser (light peak power of the order of MW compared to mW of CW light) indicates that reaction paths other than energy transfer and/or non-linear effects might be present,[33] possibly elicited by the high density of orbitals due to the straps. For this reason, only values obtained with the steady-state technique were reported in Table 2, with minor differences observed between the Φ_Δ for porphyrins **4**.

Nevertheless, with both values observed as close to 1, a lack of significant deviation from planarity was indicated for the pair of isomers. Previous investigation of redaporfin atropisomers has indicated that distribution of polar substituents relative to the porphyrin macrocycle influences cellular internalization,[4] thus, insight into porphyrin shape is critical.

Table 2. Photophysical and photochemical properties of strapped porphyrins.

Strapped porphyrin	λ_{Soret} [nm]	log ε [M^{-1} cm^{-1}]	Φ_F	Φ_Δ
cis-αβ-**4**	424	5.32	0.084	1.22[b]
cis-αα-**4**	424	5.36	0.095	1.06[b]
cis-αβ-**5**	428	4.33	0.067	–
cis-αα-**5**	428	4.91	0.089	–
trans-αβ-**6**[a]	424	3.75	0.064	0.98 ± 0.01
cis-αα-**6**[a]	434	4.71	0.111	0.76 ± 0.06

[a] λ_{Soret} and ε recorded in THF. All other measurements recorded in DMSO. [b] Single representative experiment.

Cellular Internalization

Strapped porphyrin cell-internalization varied in two cancer cell lines depending on configuration. Picket fence porphyrin atropisomer internalization has been observed to vary according to $\alpha_4 > \alpha_3\beta > \alpha_2\beta_2 > \alpha\beta\alpha\beta$.[4]

Research Article
doi.org/10.1002/ejoc.202201453

The strapped porphyrins **6** were selected for evaluation as they shared higher DMSO solubility. Measurement of strapped porphyrin fluorescence from the supernatant obtained after cell lysis confirmed the enhanced uptake (>90 fold increase) of strapped-porphyrin internalization *cis*-αα-**6** relative to *trans*-αβ-**6** when both short (4 h) and long (24 h) incubation times were used (Figure 4A,B). At the porphyrin concentration evaluated (4 μM), there was nearly a complete absence of *trans*-αβ-**6** cell internalization observed in both cell lines.

In terms of distribution of polar substituents relative to the porphyrin macrocycle, the *cis*-αα, *cis*-αβ and *trans*-αβ isomers of double strapped porphyrins are analogues to porphyrin atropisomers α_4, $\alpha_2\beta_2$, and αβαβ, respectively. The increased cell-internalization of *cis*-αα relative to *trans*-αβ follows the pattern of uptake previously observed with redaporfin atropisomers; enhanced internalization for the α_4 atropisomer relative to the other atropisomers of the drug mixture.[4] As with the α_4 atropisomer, the *cis*-αα polar substituents are oriented to one side of the porphyrin macrocycle hydrophobic core. This induces amphipathicity which is expected to confer an advantage for passive membrane permeation. The presence of straps effectively locks this favorable configuration to ensure stability against interconversion. Incorporation of the α_4 molecular configuration proved successful as a transferable motif for the design of macromolecules with enhanced cell-internalization. This is particularly critical for strapped-systems where molecular weight (>1k Da) tends to exceed that of unstrapped counterparts (<1 kDa).

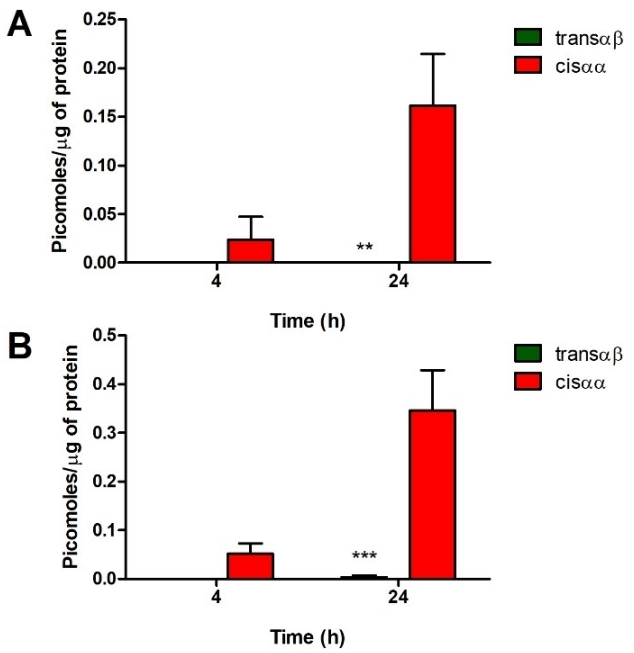

Figure 4. Cellular internalization of strapped porphyrins. (A,B) Quantification of strapped porphyrins **6** in the supernatant of cancer cells obtained after cell lysis. Cancer cells were incubated with strapped porphyrins **6** for indicated timepoints followed by cell lysis of (A) 4T1 and (B) CT26 cells. Bars indicate the mean ± SEM of three independent experiments with statistical significance evaluated using two-way ANOVA in comparison to the *cis*-αα porphyrin, * $p<0.05$ ** $p<0.01$ and *** $p<0.001$.

Conclusion

Restrictive strap moieties effectively stabilized a favorable atropisomer configuration to enhance cell-internalization. A series of double strapped porphyrins were prepared using direct condensation reactions which favor the formation of *cis*-isomers. Characterization of isomer configuration was assisted with NMR spectroscopy and X-ray crystallography methods. Photophysical evaluation indicated relative planarity of strapped porphyrin isomers and the appropriate method to evaluate cellular uptake. Internalization was assessed across two cancer cell lines and revealed enhanced membrane passage of the *cis*-αα isomer. This isomer was formed in greatest yield following the Lindsey condensation method. Lack of interconversion at elevated temperatures confirmed *cis*-αα stability. The structure of *cis*-αα is analogous to the α_4 atropisomer of redaporfin in terms of distribution of polar substituents. Straps concomitantly prevented atropisomer interconversion and enforced a structure which would potentiate cellular uptake. This development of strategies, which can impose high interconversion barriers while exploiting the benefit of a single atropisomer configuration, endorses the potential of atropisomer drugs candidates.

Experimental Section

General synthetic and analytical methods: All chemicals were commercially sourced and used without further purification. Analytical TLC was performed using silica gel 60 (fluorescence indicator F254, pre-coated sheets, 0.2 mm thick, 20 cm×20 cm; Merck) plates and visualized by UV irradiation (λ = 254 nm). Column chromatography was carried out using Fluka Silica Gel 60 (230–400 mesh; Merck). NMR spectra were recorded on a Bruker AV 600, Bruker Advance III 400 MH or a Bruker DPX400 400 MHz or an Agilent 400 spectrometer. Accurate mass measurements (HRMS) were carried out using a Bruker microTOF–Q™ ESI-TOF mass spectrometer. Mass spectrometry was performed with a Q-Tof Premier Waters MALDI quadrupole time-of-flight (Q-TOF) mass spectrometer equipped with Z-spray electrospray ionization (ESI) and matrix-assisted laser desorption ionization (MALDI) sources in positive mode with *trans*-2-[3-(4-*tert*-butylphenyl)-2-methyl-2-propenylidene]malononitrile as the matrix. ESI mass spectra were acquired in positive modes as required, using a Micromass time-of-flight mass spectrometer (TOF) interfaced to a Waters 2960 HPLC or a Bruker microTOF–Q III spectrometer interfaced to a Dionex UltiMate 3000 LC. Atmospheric pressure chemical ionization (APCI) experiments were performed on a Bruker microTOF-Q III spectrometer interfaced to a Dionex UltiMate 3000 LC. Melting points were measured using an automated melting point meter, SMP50 (Stuart), and are uncorrected.

Dialdehyde 1

1,6-Bis(2-formyl-4-nitro-phenoxy)hexane: 5-Nitrosalicylaldehyde (1.0856 g, 6.5 mmol) and K_2CO_3 (716.2 mg. 5.18 mmol) were dried under high vacuum. Anhydrous DMF (8 mL) was added and the solution was stirred at 60 °C for 1 h prior to the addition of 1,5-dibromohexane (417.2 mg, 1.71 mmol). The reaction mixture was stirred at 80 °C under Ar overnight. DMF

Research Article
doi.org/10.1002/ejoc.202201453

was evaporated by high vacuum distillation. The residue was washed with CH_2Cl_2 and EtOH (250 mL). Solvent was removed under reduced pressure. The resulting residue was recrystallized three times from EtOH (75 °C) to yield a pale white solid (663.3 mg, 1.59 mmol, 95 %). M.p. = 205 °C; R_f = 0.80 (EtOAc:*n*-hexane, 9 : 1); ^{1}H NMR (600 MHz, DMSO-d_6): δ = 10.32 (s, 2H, CHO), 8.48 (dd, J = 9.2, 3.0 Hz, 2H, Ar–H), 8.40 (d, J = 3.0 Hz, 2H, Ar–H), 7.47 (d, J = 9.3 Hz, 2H, Ar–H), 4.32 (s, 4H, CH_2), 1.89–1.85 (m, 4H, CH_2), 1.56 ppm (s, 4H, CH_2); ^{13}C NMR (151 MHz, DMSO-d_6): δ = 188.02, 187.98, 165.06, 140.66, 130.98, 123.92, 123.55, 114.70, 69.65, 28.09, 24.85 ppm; HRMS (APCI): *m/z* calc. for $C_{20}H_{20}N_2O_8$ $[M]^+$: 416.1220; found $[M + Na^+]$ 417.1292.

Dialdehyde 2

1,3-Bis(2-formyl-4-nitro-phenoxy)xylene: 5-Nitrosalicylaldehyde (503.2 mg, 3.01 mmol) and K_2CO_3 (278.8 mg. 2.02 mmol) were dried under high vac. Anhydrous DMF (3.5 mL) was added and the solution was stirred at 60 °C for 1 h prior to the addition of α,α′-dibromo-*m*-xylene (263.9 mg, 0.0.997 mmol). The reaction mixture was stirred at 80 °C under Ar overnight. DMF was evaporated by high vacuum distillation. The residue was washed with CH_2Cl_2 and EtOH (100 mL). Solvent was removed under reduced pressure. The resulting residue recrystallized three times from EtOH (75 °C) to yield a pale white solid (181 mg, 0.41 mmol, 42 %). M.p. = 191–193 °C; R_f = 0.17 (CH_2Cl_2); ^{1}H NMR (600 MHz, $CDCl_3$): δ = 10.49 (s, 2H, CHO), 8.73 (d, J = 2.9 Hz, 2H, Ar–H), 8.43 (dd, J = 9.2, 2.9 Hz, 2H, Ar–H), 7.57–7.45 (m, 4H, Ar–H), 7.19 (d, J = 9.2 Hz, 2H, Ar–H), 5.36 ppm (s, 4H, CH_2); ^{13}C NMR (151 MHz, $CDCl_3$): δ = 187.41, 187.37, 164.46, 142.10, 135.73, 130.77, 129.92, 128.04, 126.38, 125.14, 113.48, 71.24 ppm; HRMS (ESI): *m/z* calc. for $C_{22}H_{16}N_2O_8$ $[M]^+$: 436.0907; found $[M + Na^+]$ 459.0803.

Dialdehyde 3

Dimethyl 4,4′-((1,4-phenylenebis(methylene))bis(oxy))bis(3-formylbenzoate): Methyl 3-formyl-4-hydroxybenzoate (1 g, 5.55 mmol) and K_2CO_3 (920.44 mg. 6.66 mmol) were dried under high vacuum. Anhydrous DMF (15 mL) was added and the solution was stirred at 60 °C for 1 h prior to the addition of α-α′-dibromo-*p*-xylene (585.99 mg, 2.22 mmol). The reaction mixture was stirred at 80 °C under Ar overnight. DMF was evaporated by high vacuum distillation. The residue was washed with CH_2Cl_2 followed by acetone (100 mL). Solvent was removed under reduced pressure to yield a pale-yellow solid (1.9565 g, 4,.231 mmol, 96 %). M.p. = 219–221 °C; R_f = 0.17 (CH_2Cl_2); ^{1}H NMR (400 MHz, $CDCl_3$): δ = 10.53 (s, 2H, CHO), 8.53 (d, J = 2.3 Hz, 2H, Ar–H), 8.23 (dd, J = 8.8, 2.3 Hz, 2H, Ar–H), 7.50 (s, 4H, Ar–H), 7.11 (d, J = 8.8 Hz, 2H, Ar–H), 5.29 (d, J = 3.2 Hz, 4H, CH_2), 3.91 ppm (s, 6H, CH_3); ^{13}C NMR (101 MHz, $CDCl_3$): δ = 188.70, 165.93, 163.71, 137.10, 135.77, 135.53, 130.79, 127.84, 112.77, 70.41, 52.22, 30.93 ppm; HRMS (ESI): *m/z* calc. for $C_{26}H_{22}O_8$ $[M]^+$: 462.1315; found $[M + Na^+]$ 485.1233.

Strapped porphyrins 4: 1,6-Bis(2-formyl-4-nitro-phenoxy)hexane (1.09 g, 2.62 mmol) was dissolved in CH_2Cl_2 (750 mL) and pyrrole (351.26 mg, 5.24 mmol) was added to the solution. The mixture was purged with Ar for 15 minutes prior to the addition of $BF_3 \cdot OEt_2$ (520.15 mg, 3.66 mmol). The reaction mixture was shielded from light and stirred overnight at rt. DDQ (2.082 g, 9.17 mmol) was added to the solution and stirred for an additional 2 h. A color change of orange/red to black/purple was observed. The mixture was quenched by the addition of TEA (318.14 mg, 3.14 mmol). The solution volume was reduced to half by removal of solvent under reduced pressure. The resulting crude residue was filtered through a short silica column (CH_2Cl_2:EtOAc, 98 : 2, v/v). The mixture of two strapped porphyrins which was separated by a second column (CH_2Cl_2:*n*-hexane, 98 : 2, v/v).

***cis*-αβ-4**: Removal of solvent under reduced pressure, from the first fraction, ***cis*-αβ-4**, yielded a red solid (6 mg, 0.586 mmol, 0.22 %). M.p. > 300 °C; R_f = 0.45 (CH_2Cl_2:EtOAc, 98 : 2, v/v); ^{1}H NMR (600 MHz, $CDCl_3$/TFA-d_1 excess): δ = 9.18 (s, 8H, CH_{beta}), 8.84 (d, J = 9.2 Hz, 4H, Ar–H), 8.80 (s, 4H, Ar–H), 7.49 (d, J = 9.3 Hz, 4H, Ar–H), 4.13 (s, 1H, CH_2), 3.91 (s, 4H, CH_2), 1.11 (d, J = 35.7 Hz, 4H, CH_2), 0.66 (s, 4H, CH_2), 0.43–0.26 ppm (m, 8H, CH_2); ^{13}C NMR (151 MHz, $CDCl_3$/ TFA-d_1 excess): δ = 185.59, 164.04, 159.60, 159.32, 159.05, 158.77, 146.01, 144.57, 141.30, 130.84, 130.34, 128.69, 128.33, 117.26, 116.70, 115.36, 113.47, 112.49, 111.58, 70.26, 29.85, 28.81, 26.34, 14.25 ppm; UV-vis (DMSO) λ_{max} ($M^{-1}\,cm^{-1}$) = 424 (210,300), 516 (11,330), 590 (3513), 647 nm (1237); HRMS (MALDI LD$^+$): *m/z* calc. for $C_{56}H_{46}N_8O_{12}$ $[M]^+$: 1022.3235; found 1022.3198.

***cis*-αα-4**: The crude second fraction (58.7 mg, 0.0574 mmol) was dissolved in CH_2Cl_2 (20 mL) and stirred at rt. $Zn(OAc)_2 \cdot 2H_2O$ (126.2 mg, 0.575 mmol) dissolved in MeOH (3 mL), was added to the solution and stirred overnight at rt. Removal of solvent occurred under reduced pressure. The resulting residue was dissolved in CH_2Cl_2 and washed sequentially with H_2O (×3). The organic layer was dried over $MgSO_4$ and the solvent removed under reduced pressure to yield a red solid. Recrystallization from EtOAc (75 °C) was set-up to remove 1,6-bis(2-formyl-4-nitro-phenoxy)hexane **1** impurity. Cooling of the solution to rt resulted in dialdehyde **1** precipitation which was separated by filtration. EtOAc of the filtrate was removed under reduced pressure. Column chromatography with CH_2Cl_2:EtOAc (99 : 1, v/v) yielded pure Zn strapped porphyrin **4**. M.p. > 300 °C; R_f = 0.16 (CH_2Cl_2); HRMS (ESI): *m/z* calc. for $C_{56}H_{46}N_8O_{12}Zn$ $[M]^+$: 1084.2370, found $[M+H^+]$ 1085.2443. Removal of Zn was achieved by stirring in CH_2Cl_2 (20 mL) and TFA (1.5 mL) at rt for 1 h. The solvent was removed under reduced pressure and the resulting residue dissolved in CH_2Cl_2, washed sequentially with sat. aq. $NaHCO_3$ twice and deionized H_2O. The organic layer was dried over $MgSO_4$ and the solvent removed under reduced pressure. Column chromatography (CH_2Cl_2) purification was used to yield a red solid, ***cis*-αα-4** (14 mg, 0.137 mmol, 0.52 %). M.p. > 300 °C; R_f = 0.29 (CH_2Cl_2:EtOAc, 98 : 2, v/v); ^{1}H NMR (400 MHz, $CDCl_3$/ TFA excess): δ = 9.06 (s, 4H, Ar–H), 8.95 (s, 1H, CH_{beta}), 8.92–8.85 (m, 4H, Ar–H), 8.78 (s, 4H, CH_{beta}), 7.62 (d, J = 9.4 Hz, 4H, CH_2), 4.30 (t, J = 9.4 Hz, 4H, CH_2), 4.23–4.14 (m, 4H, CH_2), 1.48 (d, J = 13.2 Hz, 4H, CH_2), 1.02 (s, 4H, CH_2), 0.88–0.64

(m, 8H, CH_2), −1.69 ppm (d, J = 38.8 Hz, 2H, NH); ^{13}C NMR (101 MHz, $CDCl_3$/ TFA excess): δ = 164.27, 146.18, 145.62, 140.68, 139.80, 132.65, 130.11, 129.14, 128.32, 125.70, 116.60, 116.03, 115.00, 113.38, 113.21, 112.17, 70.66, 29.62, 28.61, 26.03 ppm; UV-vis (DMSO) λ_{max} ($M^{-1}cm^{-1}$) = 424 (227,600), 516 (12,090), 590 (3469), 647 nm (1100); HRMS (MALDI LD$^+$): *m/z* calc. for $C_{56}H_{46}N_8O_{12}$ $[M]^+$: 1022.3235; found 1022.3193.

Strapped porphyrins 5: 1,3-Bis(2-formyl-4-nitrophenoxy)xylene (904.1 mg, 2.07 mmol) was dissolved in propionic acid (40 mL) at 100 °C. An addition of pyrrole (277.75 mg, 4.14 mmol) was made to the solution. The mixture was shielded from light and refluxed at 150 °C for 4 h. A color change of yellow to black/purple was observed. $CH_3CH_2CO_2H$ was evaporated by distillation under high vacuum. The resulting crude residue was filtered through a short silica column (CH_2Cl_2). The complete purification was performed through a repetitive silica gel column chromatography. An initial column with CH_2Cl_2: EtOAc (98 : 2, v/v) separated the *trans*-αβ-5 as the first fraction and a mixture of the *cis* strapped porphyrins which was followed by a second column ($CHCl_3$:EtOAc 96 : 4, v/v) to separate the mixture.

***trans*-αβ-5**: The first fraction which eluted from the column was dried under reduced pressure to yield a red solid, *trans*-αβ-5, (2.0 mg, 0.018 mmol, 0.1 %). M.p. > 300 °C; R_f = 0.29 (CH_2Cl_2: EtOAc, 98 : 2, v/v); ^{1}H NMR (400 MHz, CD_3CN/TFA excess): δ = 9.76 (d, J = 2.8 Hz, 4H, Ar–H), 8.97 (s, 8H, CH_{beta}), 8.59 (dd, J = 9.0, 2.8 Hz, 4H, Ar–H), 7.00 (d, J = 9.0 Hz, 4H, Ar–H), 6.47 (t, J = 7.6 Hz, 2H, Ar–H), 5.89 (dd, J = 7.6, 1.6 Hz, 4H, Ar–H), 5.10 (d, J = 3.7 Hz, 2H, Ar–H), 3.85 ppm (s, 8H CH_2); ^{13}C NMR (101 MHz, CD_3CN/TFA excess): δ = 162.90, 142.08, 141.68, 140.45, 133.68, 132.56, 128.09, 127.95, 127.07, 126.56, 123.31, 118.96, 116.22, 116.20, 116.19, 116.13, 116.09, 116.07, 116.05, 116.03, 113.43, 113.38, 113.36, 113.34, 113.30, 110.51, 71.31, 29.71, 29.39, 29.27, 22.78, 13.10, 12.94 ppm; HRMS (MALDI LD$^+$): *m/z* calc. for $C_{60}H_{38}N_8O_{12}$ $[M]^+$: 1062.2609; found 1062.2638.

***cis*-αβ-5**: The first fraction which eluted from the second column was dried under reduced pressure to yield a red solid, *cis*-αβ-5, (5.6 mg, 0.053 mmol, 0.25 %). M.p. > 300 °C; R_f = 0.44 ($CHCl_3$:EtOAC, 98 : 2, v/v); ^{1}H NMR (400 MHz, CD_3CN/TFA excess): δ = 9.47 (s, 4H, CH_{beta}), 9.29 (d, J = 2.0 Hz, 4H, Ar–H), 9.21 (s, 4H, CH_{beta}), 8.89 (dd, J = 9.2, 2.7 Hz, 4H, Ar–H), 7.72 (d, J = 9.3 Hz, 4H, Ar–H), 7.22 (s, 2H, Ar–H), 6.60 (d, J = 7.3 Hz, 4H, Ar–H), 6.48 (t, J = 7.4 Hz, 2H, Ar–H), 5.28 (d, J = 9.7 Hz, 4H, CH_2), 4.78 ppm (d, J = 9.7 Hz, 4H, CH_2); UV-vis (DMSO) λ_{max} ($M^{-1}cm^{-1}$) = 427 (21,325), 519 (925), 594 (668), 647 nm (79); HRMS (MALDI LD$^+$): *m/z* calc. for $C_{60}H_{38}N_8O_{12}$ $[M]^+$: 1062.2609; found 1062.2614. It was not possible to obtain the ^{13}C NMR spectrum due to low solubility.

***cis*-αα-5**: Removal of solvent under reduced pressure, from the third fraction, yielded a red solid, cis-αα-5, (22.6 mg, 0.212 mmol, 1 %). M.p. > 300 °C; R_f = 0.67 ($CHCl_3$:EtOAc, 98 : 2, v/v), ^{1}H NMR (400 MHz, CD_3CN/TFA excess): δ = 9.18 (d, J = 2.7 Hz, 4H, Ar–H), 9.14 (s, 4H, CH_{beta}), 8.94 (dd, J = 9.2, 2.7 Hz, 4H, Ar–H), 8.87 (s, 4H, CH_{beta}), 7.90 (d, J = 9.3 Hz, 4H, Ar–H), 7.77 (s, 2H, Ar–H), 6.95 (d, J = 7.6 Hz, 4H, Ar–H), 6.89–6.82 (m, 2H, Ar–H), 5.67 (d, J = 10.0 Hz, 4H, CH_2), 5.00 ppm (d, J = 10.0 Hz, 4H, CH_2); ^{13}C NMR (101 MHz, CD_3CN/TFA excess): δ = 162.84, 146.12, 145.77, 141.63, 135.31, 134.10, 129.84, 128.82, 128.24, 127.41, 118.90, 116.07, 112.81, 110.41, 71.79 ppm; UV-vis (DMSO) λ_{max} ($M^{-1}cm^{-1}$) = 428 (81,510), 519 (5199), 594 (2105), 648 nm (1981); HRMS (MALDI LD$^+$): *m/z* calc. for $C_{60}H_{38}N_8O_{12}$ $[M]^+$: 1062.2609; found 1062.2558.

Strapped porphyrins 6

COOMe-*cis*-αα-6: Dimethyl 4,4′-[(1,4-phenylenebis(methylene)bis(oxy)]bis(3-formylbenzoate)] (2 g, 4.23 mmol) and pyrrole (0.6 mL, 8.46 mmol) were dissolved in chloroform (1.4 L) and the solution was shielded from light and purged with an Ar stream for 20 min, followed by the addition of $BF_3 \cdot OEt_2$ (730 μL, cat.). The reaction mixture was stirred at r.t. for 24 h under an Ar atmosphere. DDQ (3 g, 13.12 mmol) was added and the reaction mixture was stirred for an additional 2 h. The reaction was quenched by the addition of TEA (3 mL), and the crude product was filtered through a short silica column. The complete purification was performed through a silica gel column chromatography using CH_2Cl_2:EtOAc (50 : 1, v/v) as eluent. The first fraction was collected. Solvents were removed under reduced pressure and recrystallization from CH_2Cl_2 and ethanol was carried out to obtain the product as a purple crystalline solid (61 mg, 55.41 μmol, 1.3 %). M.p. > 300 °C; R_f = 0.33 (CH_2Cl_2: EtOAc, 50 : 1, v/v); ^{1}H NMR (600 MHz, $CDCl_3$): δ = 8.78 (s, 4H, CH_{beta}), 8.67 (d, J = 2.2 Hz, 4H, Ar–H), 8.52 (dd, J = 8.8, 2.2 Hz, 4H, Ar–H), 7.87 (s, 4H, CH_{beta}), 7.61 (d, J = 8.9 Hz, 4H, Ar–H), 5.13 (d, J = 1.1 Hz, 8H, CH_2), 3.90 (s, 12H, CH_3), −2.90 ppm (s, 2H, NH); ^{13}C NMR (151 MHz, $CDCl_3$): δ = 167.32, 163.84, 136.89, 136.74, 133.80, 132.32, 123.12, 116.89, 115.07, 52.47 ppm; UV-vis (CH_2Cl_2) λ_{max} ($M^{-1}cm^{-1}$) = 426 (288,403), 519 (10,233), 588 nm (10,233); HRMS (ESI): *m/z* calc. for $C_{68}H_{51}N_4O_{12}$ $[M]^+$: 1115.34980; found 1115.352107.

COOH-*cis*-αα-6: Strapped porphyrin **COOMe-*cis*-αα-6** (38 mg, 0.03384 mmol) was added to a 100 mL round bottom flask containing MeOH (30 mL) and THF (45 mL). KOH (0.4756 g, 8.476 mmol) dissolved in water (10 mL) was added. The reaction mixture was refluxed at 100 °C for 60 h and cooled to rt. Solvents were removed under reduced pressure and the solution was acidified to pH 5 with hydrochloric acid (1 M) to precipitate the product. Solid was isolated by filtration and washed with water (3 × 15 mL). The purple solid was oven dried for 3 days (37.5 mg, 99 %, 0.0335 mmol). M.p. > 300 °C; R_f = 0.54 (DCM: EtOH, 100 : 1, v/v); ^{1}H NMR (400 MHz, DMSO-d_6): δ = 12.94 (s, 4H, COOH), 8.72 (s, 4H, CH_{beta}), 8.53-8.50 (m, 8H, Ar–H), 8.14 (s, 4H, CH_{beta}), 7.95 (d, J = 8.8 Hz, 4H, Ar–H), 5.44 (d, J = 11.6 Hz, 4H, CH_2), 5.06 (d, J = 11.4 Hz, 4H, CH_2), −3.24 ppm (s, 2H, NH);^{13}C NMR (151 MHz, DMSO-d_6): δ = 167.65, 163.22, 136.89, 136.25, 132.53, 132.15, 128.57, 123.29, 116.93, 115.19, 74.14.ppm; UV-vis (THF) λ_{max} ($M^{-1}cm^{-1}$) = 424 (51,287), 519 (2818), 555 nm (1096); HRMS (ESI): *m/z* calc. for $C_{64}H_{43}N_4O_{12}$ $[M+H]^+$: 1059.287199; found 1059.284924.

COOMe-*trans*-αβ-6: Dimethyl 4,4′-[(1,4-phenylenebis(methylene)bis(oxy)]bis(3-formylbenzoate)) (700 mg, 1.51 mmol) was added to a 100 mL flask and dissolved in propionic acid (50 mL). The mixture was heated to 100 °C, and pyrrole (209 μL,

3.03 mmol) was added dropwise. The reaction mixture was shielded from light and left stirring under reflux at 150 °C for 3 h. After reaction completion, propionic acid was removed through vacuum distillation and the crude product was filtered through a short silica column using CH_2Cl_2:MeOH (99:1). Complete purification was performed via column chromatography using CH_2Cl_2/EtOH (gradient 99.9:0.1 to 98:2). After removing the solvents under reduced pressure, the desired product was obtained as a purple crystalline solid (8 mg, 7.17 μmol, 0.5 %). M.p > 300 °C; R_f = 0.27 (CH_2Cl_2: EtOH, 100:1, v/v); ^{1}H NMR (600 MHz, $CDCl_3$): δ = 9.48 (d, J = 2.2 Hz, 4H, Ar–H), 8.69 (s, 8H, CH_{beta}), 8.32 (dd, J = 8.4, 2.2 Hz, 4H, Ar–H), 6.78 (d, J = 8.5 Hz, 4H, Ar–H), 4.19 (s, 8H, Ar–H), 4.10 (s, 12H, CH_3), 3.94 (s, 8H, CH_2), −0.26 ppm (s, 2H, NH); ^{13}C NMR (151 MHz, $CDCl_3$) δ = 167.75, 162.69, 134.37, 132.73, 130.53, 130.40, 125.19, 122.53, 113.15, 112.40, 69.71, 52.63.ppm; UV-vis ($CHCl_3$) λ_{max} ($M^{-1}cm^{-1}$) = 426 (58,884), 521 (4467), 598 nm (1950); HRMS (APCI): *m/z* calc. for $C_{68}H_{51}N_4O_{12}$ $[M]^+$: 1115.34980; found 1115.347064.

COOH-*trans*-αβ-6: Strapped porphyrin COOMe-*trans*-αβ-6 (11 mg, 9.8 μmol) was added to a 100 mL round bottom flask containing MeOH (20 mL) and THF (30 mL). KOH (120 mg, 2.15 mmol) dissolved in water (10.0 mL) was added. The reaction mixture was refluxed at 100 °C for 60 h and cooled to rt. Solvents were removed under reduced pressure and the solution was acidified to pH 5 with hydrochloric acid (1 M) to precipitate the product. Solid was isolated by filtration as a purple solid (10 mg, 96 %, 9.4 μmol). M.p. > 300 °C; R_f = 0.54 (CH_2Cl_2: EtOH, 100:1, v/v); ^{1}H NMR (400 MHz, THF-d_8) δ = 10.86 (s, 4H, COOH), 9.48 (d, J = 2.0 Hz, 4H, Ar–H), 8.71 (s, 8H, CH_{beta}), 8.31 (dd, J = 8.4, 1.9 Hz, 4H, Ar–H), 6.91 (d, J = 8.5 Hz, 4H, Ar–H), 4.23 (s, 8H, Ar–H), 4.00 (s, 8H, CH_2), −0.15 (s, 2H, NH) ppm; ^{13}C NMR (101 MHz, THF-d_8) δ = 168.04, 163.41, 145.23, 135.54, 133.40, 131.49, 131.24, 131.15, 125.65, 123.96, 114.36, 112.99, 108.57, 108.48, 107.12, 104.65, 70.12 ppm; UV-vis (THF) λ_{max} ($M^{-1}cm^{-1}$) = 434 (5623), 527 (417), 607 nm (151); HRMS (ESI): *m/z* calc. for $C_{64}H_{43}N_4O_{12}$ $[M+H]^+$: 1059.287199; found 1059.287199.

X-Ray Crystallography: Crystals of the separated strapped porphyrins were grown by the following procedures: samples were dissolved in dichloromethane and layered with hexane. Samples were left to diffuse over the course of one week and crystals appeared at the side of the crystallization tube. Diffraction data were collected for each of the two samples on a Bruker APEX-II DUO instrument, with an Oxford Cobra Cryosystem low temperature device using a MiTeGen micromount. Using the OLEX2 Software Package,[34] the structure was solved with the SHELXT structure solution program[35] using Intrinsic Phasing and refined with the SHELXL refinement package[36] with Least Squares minimization. Data reductions were performed with the Bruker APEX3 package[37] and SAINT;[38] structures were solved with SHELXT and refined with ShelXL[35] in the Shelxle GUI.[36] Data were corrected for absorption effects using the Multi-Scan method (SADABS).[39] Images were generated with OLEX2 software package.[34] Critical values related to the crystal structure refinement are in Table S1.

Deposition Numbers 2234046 (for **3**), 2223649 (for *cis*-αβ-**4**), 2223650 (for *cis*-αα-**4**), 2223651 (for COOH-*cis*-αα-**6**), 2223652 (for COOH-*trans*-αβ-**6**) contain the supplementary crystallographic data for this paper. These data are provided free of charge by the joint Cambridge Crystallographic Data Centre and Fachinformationszentrum Karlsruhe Access Structures service.

Refinement details

***cis*-αβ-4**: For the half molecules in the asymmetric unit, pyrrole hydrogens were located and refined with restraints (DFIX). One of these has disorder in one nitro group position, modelled in two positions, 63:37 % occupancy, with restraints (SADI, SIMU). There was also disorder in the hexyl chain linker (O56-C60) and this was modelled in two positions, 52:48 % occupancy, with restraints (SADI, ISOR).

***cis*-αα-4**: Disorder was seen in both 1,6-bis(4-nitrophenoxy)hexane substituents with complete disorder seen in C25-C44 (87:13 % occupancy) and disorder in the remaining nitrophenylhexyl moiety C45-C57 (78:22 % occupancy). Disorder was modelled with restraints (SADI, DFIX, SIMU and DANG). Pyrrole hydrogens were located on the difference map and refined with restraints (DFIX).

COOMe-cis-αα-6: Solvent DCM molecule disordered and modelled over 4 locations, occupancies 75:12:8:5 %, using rigid groups and restraints (SIMU, ISOR). High R(int) due to weak high angle data.

COOMe-*trans*-αβ-6: Very weak data from a poorly diffracting sample leading to a high R(int). Data limited to 0.87 Angstroms. One phenyl ester was modelled in two locations, 53:47 % occupied with geometric (SIMU) and displacement (SIMU, ISOR) restraints. PLATON SQUEEZE[40] used to subtract the diffuse solvent component resulting in the removal of 190 electrons/683 cubic Angstrom void per asymmetric unit. This is approx. 7 EtOH molecules.

Photophysical and photochemical characterization: Absorption spectra of strapped porphyrins were recorded on an Agilent Cary5000 UV-VIS-NIR spectrometer. The absorption coefficients (ε) were obtained from absorption measurements of three solutions of different concentrations, diluted from two stock solutions with independently measured masses. The slope of the plot absorption vs. concentration was used to calculate ε. Further photophysical characterization of strapped porphyrins were carried out with fluorescence emission and excitation spectra recorded on the Horiba-JY and Fluoromax4 spectrofluorometer. Strapped-porphyrin absolute values of Φ_F, obtained for each strapped porphyrin, were measured using the absolute method with a Hamamatsu Quantaurus QY absolute photoluminescence quantum yield spectrometer model C11347 (integration sphere). Solutions with absorbance < 0.1 were used. The quantum yield of singlet oxygen (Φ_Δ) was recorded using a steady-state technique exciting at 424 nm and collecting the phosphorescence of singlet oxygen between 1240 and 1340 nm on a Horiba-Jovin-Yvon Spex Fluorog 3-2.2 spectrophotometer coupled to the near-infrared Hamamatsu R5509-42

Research Article
doi.org/10.1002/ejoc.202201453

photomultiplier, cooled to 193 K in a liquid nitrogen chamber. A time-resolve technique was also used exciting the molecules with a Nd:YAG pulsed laser of 8 ns at 355 nm and the decay detected at 1270 nm using the same detector reported above. The singlet oxygen reference was phenalenone in DMSO ($\Phi_\Delta = 1$, steady-state), determined in this work, and in MEOH ($\Phi_\Delta = 0.98$, time-resolved).[41] A long-pass filter (Newport, 10LWF-1000-B, AE23) was used to avoid fluorescence from porphyrins. The quantum yields, using both techniques, were calculated using the Equation (1):

$$\Phi_\Delta = \frac{(1-10^{-A_R})}{(1-10^{-A_S})}\frac{I_S}{I_R}\Phi_\Delta^R \quad (1)$$

Where R and S are reference and sample, respectively. In the steady-state method the value of *I*is the area of the phosphorescence emission and in the time-resolved case, *I* is the slope obtained from the phosphorescence signal dependence with laser energy.

Cellular internalization in vitro: 4T1 and CT26 cells were seeded (40,000 cells/well) in 24-well plates and let to adapt for 24 h. For strapped porphyrins **6**, cells were incubated with single isomers, diluted from DMSO stock solutions, at concentration of 4 μM for 4 and 24 h. Cells were lysed (DMSO: Triton X-100, 4% (v/v)) and fluorescence detection of the supernatant was performed with a microplate reader (Biotek Synergy HT) using 420/50 nm excitation and 645/40 nm emission filters. A calibration curve of each isomer was prepared in lysis buffer in order to quantify the absolute amount of internalized isomer. Protein quantification was carried out using the Pierce™ BCA Protein Assay Kit according to the manufacturer's instructions (Thermo Scientific).

Supporting Information (see footnote on the first page of this article): Spectroscopic data of all compounds and X-ray crystallographic data.

Acknowledgements

This project has received funding from Science Foundation Ireland (SFI award 21/FFP–A/9469), the Portuguese Foundation for Science and Technology (FCT project UID/QUI/00313/2019) and the European Union's Horizon 2020 research and innovation program under the Marie Skłodowska-Curie grant agreement number 764837 (Polythea-How light can save lives). This work was also supported by the Higher Education Authority and the Department of Further and Higher Education, Research, Innovation and Science (Ireland). F.S. Schaberle thanks FCT for his grant (PTDC/QUI-OUT/0303/2021_3D-CANCER). Open Access funding provided by IReL.

Conflict of Interest

The authors declare no conflict of interest.

Data Availability Statement

The data that support the findings of this study are available in the supplementary material of this article.

Keywords: atropisomerism · drug design · photodynamic therapy · porphyrins · photochemistry

[1] S. R. LaPlante, L. D. Fader, K. R. Fandrick, D. R. Fandrick, O. Hucke, R. Kemper, S. P. F. Miller, P. J. Edwards, *J. Med. Chem.* **2011**, *54*, 7005–7022.
[2] S. R. LaPlante, P. J. Edwards, L. D. Fader, A. Jakalian, O. Hucke, *ChemMedChem* **2011**, *6*, 505–513.
[3] a) J. S. Albert, C. Ohnmacht, P. R. Bernstein, W. L. Rumsey, D. Aharony, B. B. Masek, B. T. Dembofsky, G. M. Koether, W. Potts, J. L. Evenden, *Tetrahedron* **2004**, *60*, 4337–4347; b) P. Eveleigh, E. C. Hulme, C. Schudt, N. J. Birdsall, *Mol. Pharmacol.* **1989**, *35*, 477–483; c) S. T. Toenjes, M. Basilaia, J. L. Gustafson, *Future Med. Chem.* **2021**, *13*, 443–446.
[4] C. Donohoe, F. A. Schaberle, F. M. S. Rodrigues, N. P. F. Gonçalves, C. J. Kingsbury, M. M. Pereira, M. O. Senge, L. C. Gomes-da-Silva, L. G. Arnaut, *J. Am. Chem. Soc.* **2022**, *144*, 15252–15265.
[5] a) H. Ogoshi, H. Sugimoto, Z.-i. Yoshida, *Tetrahedron Lett.* **1976**, *17*, 4481–4484; b) A. R. Battersby, D. G. Buckley, S. G. Hartley, M. D. Turnbull, *J. Chem. Soc. Chem. Commun.* **1976**, 879–881.
[6] J. E. Baldwin, T. Klose, M. Peters, *J. Chem. Soc., Chem. Commun.* **1976**, 881–883.
[7] M. O. Senge, A. Meindl, in *Fundamentals of Porphyrin Chemistry: A 21st Century Approach* (Eds.: P. J. Brothers, M. O. Senge), John Wiley & Sons, Hoboken, USA, **2022**, vol. 1, pp. 37–140.
[8] U. Simonis, F. A. Walker, P. L. Lee, B. J. Hanquet, D. J. Meyerhoff, W. R. Scheidt, *J. Am. Chem. Soc.* **1987**, *109*, 2659–2668.
[9] R. Wagner, T. Johnson, J. Lindsey, *Tetrahedron* **1997**, *53*, 6755–6790.
[10] a) T. Ishizuka, N. Grover, C. J. Kingsbury, H. Kotani, M. O. Senge, T. Kojima, *Chem. Soc. Rev.* **2022**, *51*, 7560–7630; b) T. P. Wijesekera, J. B. Paine, D. Dolphin, F. W. B. Einstein, T. Jones, *J. Am. Chem. Soc.* **1983**, *105*, 6747–6749.
[11] J. A. Wytko, E. Graf, J. Weiss, *J. Org. Chem.* **1992**, *57*, 1015–1018.
[12] J. P. Collman, R. A. Decréau, S. Costanzo, *Org. Lett.* **2004**, *6*, 1033–1036.
[13] E. Rose, Q.-Z. Ren, B. Andrioletti, *Chem. Eur. J.* **2004**, *10*, 224–230.
[14] M. Tang, Y. Liang, X. Lu, X. Miao, L. Jiang, J. Liu, L. Bian, S. Wang, L. Wu, Z. Liu, *Chem.* **2021**, *7*, 2160–2174.
[15] S. Callaghan, K. J. Flanagan, J. E. O'Brien, M. O. Senge, *Eur. J. Org. Chem.* **2020**, *2020*, 2735–2744.
[16] H. Abrahamse, M. R. Hamblin, *Biochemistry* **2016**, *473*, 347–364.
[17] M. Urbani, T. Torres, *Chem. Eur. J.* **2014**, *20*, 16337–16349.
[18] M. Ravikanth, D. Reddy, T. K. Chandrashekar, *J. Photochem. Photobiol. A* **1993**, *72*, 61–67.
[19] B. Röder, M. Büchner, I. Rückmann, M. O. Senge, *Photochem. Photobiol. Sci.* **2010**, *9*, 1152–1158.
[20] E. Davoust, R. Granet, P. Krausz, V. Carré, M. Guilloton, *Tetrahedron Lett.* **1999**, *40*, 2513–2516.
[21] L. Martínez-Crespo, J. L. Sun-Wang, A. F. Sierra, G. Aragay, E. Errasti-Murugarren, P. Bartoccioni, M. Palacín, P. Ballester, *Chem* **2020**, *6*, 3054–3070.
[22] a) A. C. Gehrold, T. Bruhn, H. Schneider, U. Radius, G. Bringmann, *J. Org. Chem.* **2015**, *80*, 12359–12378; b) A. C. Gehrold, T. Bruhn, G. Bringmann, *J. Org. Chem.* **2016**, *81*, 1075–1088.
[23] a) Q. Liu, X. Zhou, H. Liu, X. Zhang, Z. Zhou, *Org. Biomol. Chem.* **2015**, *13*, 2939–2946; b) Q. Liu, J. Zhang, M. Tang, Y. Yang, J. Zhang, Z. Zhou, *Org. Biomol. Chem.* **2018**, *16*, 7725–7736.
[24] A. Osuka, F. Kobayashi, K. Maruyama, *Bull. Chem. Soc. Jpn.* **1991**, *64*, 1213–1225.
[25] S. Callaghan, M. O. Senge, *Photochem. Photobiol. Sci.* **2018**, *17*, 1490–1514.
[26] A. Charisiadis, A. Bagaki, E. Fresta, K. T. Weber, G. Charalambidis, C. Stangel, A. G. Hatzidimitriou, P. A. Angaridis, A. G. Coutsolelos, R. D. Costa, *ChemPlusChem* **2018**, *83*, 254–265.
[27] D. Reddy, T. K. Chandrashekar, *J. Chem. Soc. Dalton Trans.* **1992**, 619–625.
[28] J. S. Lindsey, I. C. Schreiman, H. C. Hsu, P. C. Kearney, A. M. Marguerettaz, *J. Org. Chem.* **1987**, *52*, 827–836.

[29] A. D. Adler, F. R. Longo, J. D. Finarelli, J. Goldmacher, J. Assour, L. Korsakoff, *J. Org. Chem.* **1967**, *32*, 476–476.
[30] M. Momenteau, J. Mispelter, B. Loock, E. Bisagni, *J. Chem. Soc. Perkin Trans. 1* **1983**, 189–196.
[31] J. E. Baldwin, M. J. Crossley, T. Klose, E. A. O Rear, M. Peters, *Tetrahedron* **1982**, *38*, 27–39.
[32] C. J. Kingsbury, M. O. Senge, *Coord. Chem. Rev.* **2021**, *431*, 213760.
[33] a) P. R. Ogilby, C. S. Foote, *J. Am. Chem. Soc.* **1982**, *104*, 2069–2070; b) R. Schmidt, *Photochem. Photobiol.* **2006**, *82*, 1161–1177.
[34] O. V. Dolomanov, L. J. Bourhis, R. J. Gildea, J. A. K. Howard, H. Puschmann, *J. Appl. Crystallogr.* **2009**, *42*, 339–341.
[35] G. Sheldrick, *Acta Crystallogr. Sect. A* **2015**, *71*, 3–8.
[36] G. Sheldrick, *Acta Crystallogr. Sect. C* **2015**, *71*, 3–8.
[37] Bruker APEX3 v2017.3-0., Bruker AXS Inc, Madison, WI, USA, **2017**.
[38] Bruker SAINT v8.38 A., Bruker AXS Inc, Madison, WI, USA, **2018**.
[39] L. Krause, R. Herbst-Irmer, G. M. Sheldrick, D. Stalke, *J. Appl. Crystallogr.* **2015**, *48*, 3–10.
[40] A. L. Spek, *Acta Crystallogr.* **2015**, *C71*, 9–18.
[41] R. Schmidt, C. Tanielian, R. Dunsbach, C. Wolff, *J. Photochem. Photobiol. A* **1994**, *79*, 11–17.

Manuscript received: December 10, 2022
Revised manuscript received: January 12, 2023
Accepted manuscript online: January 13, 2023